

**A Proposal for a Three Detector
Short-Baseline Neutrino Oscillation Program
in the Fermilab Booster Neutrino Beam**

Part IV: Infrastructure and Civil Construction

January 8, 2015

CONTENTS

I. Introduction	1
II. Cryostats	2
A. Near Detector Cryostat	2
B. Far Detector Cryostat	11
III. Cryogenic Systems	13
IV. Requirements for Near and Far Detector Buildings	17
V. Near Detector Siting and Construction	17
VI. Far Detector Siting and Construction	19
VII. Computing Infrastructure and Software	21
A. Data Acquisition and Data Quality Monitoring	21
B. Data Storage and Processing	24
C. Data Analysis Framework and Tools	25
D. Toward an Automated Reconstruction	27
References	32

I. INTRODUCTION

The Short Baseline Neutrino program is proposed to include three Liquid Argon Time Projection Chamber detectors (LAr-TPCs) located on-axis in the Booster Neutrino Beam (BNB) as shown in Figure 1. The near detector (LAr1-ND) will be located in a new building directly downstream of the existing SciBooNE enclosure 110 m from the BNB target as also shown in Figure 2 (right). The MicroBooNE detector, which is currently in the final stages of installation, is located in the Liquid Argon Test Facility (LArTF) at 470 m. The far detector (the existing ICARUS-T600) will be located in a new building, 600 m from the target between MiniBooNE and the NO ν A near detector surface building as shown in Figure 2 (left).

The following sections address the new infrastructure required to support these detectors:

- cryostats for the near and far detectors,
- cryogenic systems for the near and far detectors,
- buildings for the near and far detectors, and
- common computing and software systems.

The infrastructure required for the the MicroBooNE detector is not described here since the detector installation will have been completed by early 2015. However, development of common computing and software systems for the SBN program can benefit significantly by the participation of MicroBooNE in the development and experience from the use of these tools on MicroBooNE data.

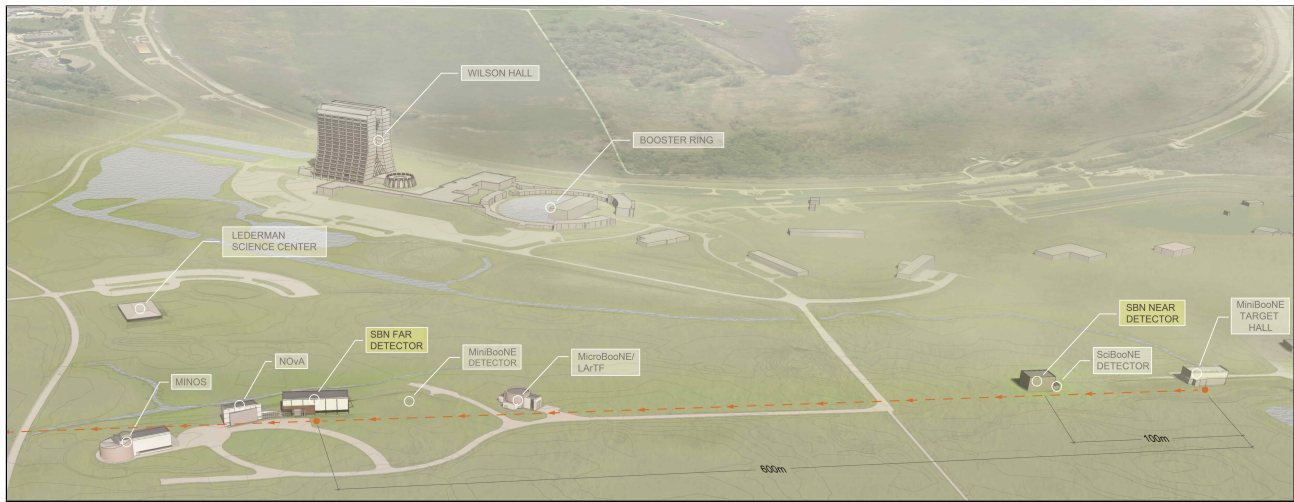


FIG. 1: Diagram of the Fermilab neutrino beamline area (looking east) showing the axis of the BNB (red dashed line) and approximate locations of the SBN detectors at 110 m, 470 m, and 600 m.

The detectors of the SBN program will need external detectors for tagging/vetoing cosmic ray muons as explained in Part 1 of this proposal. As described in Parts 2 and 3 the conceptual designs for cosmic taggers the near and far detectors are being developed. While these concepts were developed independently and described separately, it is likely that the realization of these systems will be managed as a joint project with a common underlying design. The Collaborations have made provisions in their funding requests for the necessary resources.

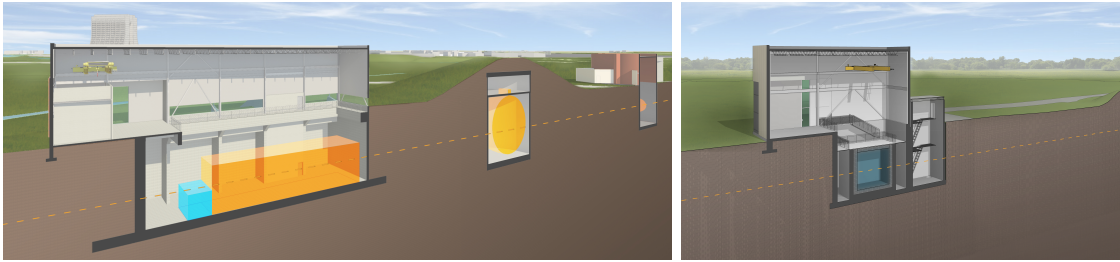


FIG. 2: *Cross-sectional views of a design concept for the far detector building (left) and near detector building (right). In the left view the existing enclosures for the MiniBooNE and MicroBooNE detectors are also seen.*

The SBN program provides an excellent opportunity for a collaborative effort on the design of LAr-TPC infrastructure between the recently formed LAr Cryogenic engineering groups at CERN and Fermilab along with engineering resources within INFN. These teams are also collaborating on developments for other short and mid-term projects leading to a long-baseline neutrino facility. The following two sections describe the cryostat and cryogenic needs for the near and far detectors.

II. CRYOSTATS

A. Near Detector Cryostat

The near detector will use a membrane tank technology to contain the base design of 220 tons of LAr equivalent to about 158 m^3 . The design is based on a scaled up version of the LBNE 35 Ton Prototype. The cryostat will be housed in a dedicated building next to the existing SciBooNE hall where the cryogenic system components will be located. The two buildings will be connected with an underground tunnel spanning about 9 feet. The cryostat will use a steel outer supporting structure with a metal liner inside to isolate the insulation volume. An alternative that was considered was a concrete supporting structure with vapor barrier and heating elements embedded in the concrete to control the temperature.

The scope of the Near Detector cryostat subsystem includes the design, procurement, fabrication, testing, delivery and oversight of a cryostat to contain the liquid argon and the TPC. This section describes a reference design, whose scope encompasses the following components:

- steel outer supporting structure,
- main body of the membrane cryostat (sides and floor),
- top cap of the membrane cryostat.

A membrane cryostat design commonly used for liquefied natural gas (LNG) storage and transportation will be used. In this vessel a stainless steel membrane contains the liquid cryogen. The pressure loading of the liquid cryogen is transmitted through rigid foam insulation to the surrounding outer support structure, which provides external support. The membrane is corrugated to provide strain relief resulting from temperature related expansion and contraction. The vessel is completed with a top cap that uses the same technology.

Two membrane cryostat vendors are known: GTT (Gaztransport & Technigaz) from France and IHI (Ishikawajima-Harima Heavy Industries) from Japan. Each one is technically capable of delivering a membrane cryostat that meets the design requirements for the Near Detector. To provide clarity, only one vendor is represented in this document, GTT; this is for informational purposes only. Figure 3 shows a 3D model of the GTT membrane and insulation design.

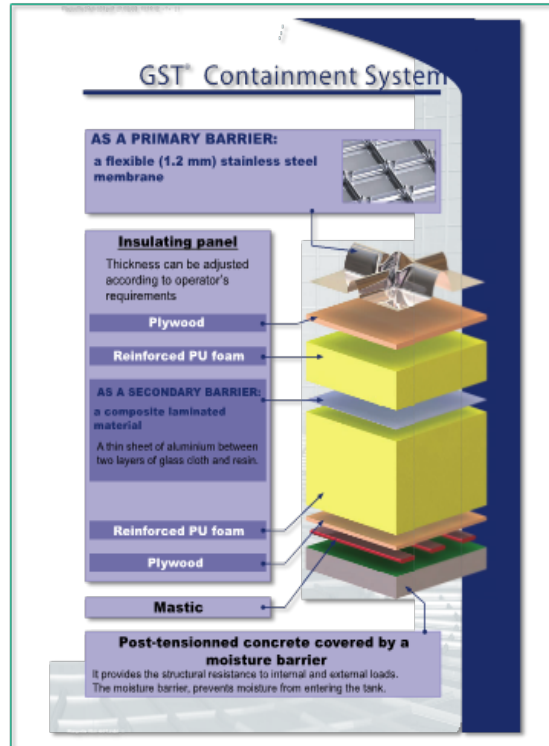


FIG. 3: Exploded view of the membrane cryostat technology.

Cryostat Design

The conceptual reference design for the Near Detector cryostat is a rectangular vessel measuring 6.38 m in length (parallel to the beam direction), 5.17 m in width, and 4.80 m in height; containing a total mass of 220 tons of liquid argon. Figure 4 shows a 3D view of the Near Detector cryostat with a neck and two main plates constituting the top: plate A and plate B. Two cold penetrations are located on plate A; all the other penetrations are located on plate B. To minimize the contamination from warm surfaces, the liquid argon level touches the membrane underneath top plate A. The gas is all contained in the neck region underneath plate B. An alternative design is being considered with a single removable plate for the top. The TPC could be directly hung from underneath this top plate. In this case the gas ullage will all be contained over the liquid argon bath.

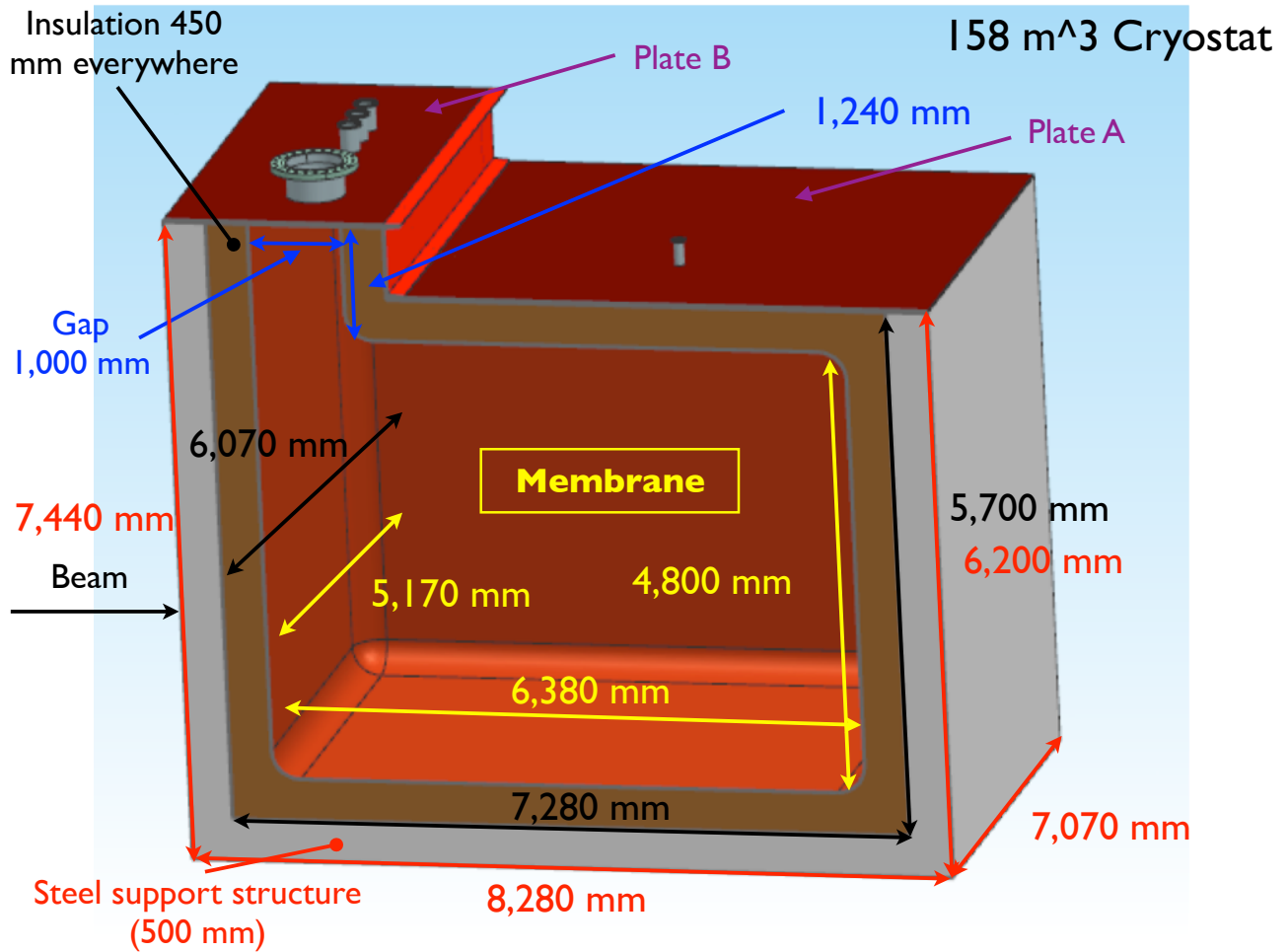


FIG. 4: A 3D view of the LAr1-ND cryostat using membrane technology.

Design parameters

This design is meant also to test technical solutions that may be of interest for the Long Baseline Neutrino program as well. The use of a cold ullage (< 100 K) to lower the impurities in the gas region, and of a LAr pump outside the cryostat to minimize the effect of noise, vibration and microphonics to the TPC inside the LAr are Value Engineering studies for the Long Baseline program performed in synergy with the LBNF cryostat and cryogenics team.

The design parameters for the Near Detector cryostat are listed in Table I.

Insulation system and secondary membrane

The membrane cryostat requires insulation applied to all internal surfaces of the outer support structure and roof in order to control the heat ingress and hence required refrigeration heat load. Choosing a reasonable, maximum insulation thickness of 0.45 m and given an average thermal conductivity coefficient for the insulation material of 0.0283 W/(m·K), the heat input

Design Parameter	Value
Total Cryostat volume	166 m ³
Total LAr volume	158 m ³
Liquid argon total mass	220,000 kg
Inner dimensions of the cryostat	6.38 m (L) x 5.17 m (W) x 4.80 m (H)
Depth of liquid argon	4.80 m (5% ullage all in the neck region)
Insulation	0.45 m Polyurethane foam
Primary membrane	1.2 mm thick SS 304L corrugated stainless steel
Secondary barrier system	0.07 mm thick aluminum between fiberglass cloth. Overall thickness is 1 mm located between insulation layers.
Outer support structure	Steel enclosure with metal liner to isolate the outside from the insulation space
Liquid argon temperature	88 ± 1°K
Operating gas pressure	Positive pressure. Nominally 70 mbar (~1psig)
Vacuum	No vacuum
Design pressure	350 mbar (~5 psig) + LAr head
Design temperature	77°K (liquid nitrogen temperature for flexibility)
Temperature of all surfaces in the ullage during operation	100°K
Minimize noise/vibration/microphonics inside cryostat	LAr pump preferably outside the cryostat
Leak tightness	1 × 10 ⁻⁶ mbar ℓ s ⁻¹
Heat leak	< 15 W/m ²
Lifetime	10 years (5 years of run + 5 years of potential upgrade)
Thermal cycles	20 complete cycles (cool down and total warm up)

TABLE I: *Design parameters for the Near Detector cryostat.*

from the surrounding steel is expected to be about 3 kW total. It assumes that plates A and B are both foam insulated. This is shown in Table II. The overall heat leak is then about 13 W/m².

The insulation material is a solid reinforced polyurethane foam manufactured as composite panels. The panels get laid out in a grid with 3 cm gaps between them (that will be filled with fiberglass) and fixed onto anchor bolts anchored to the support structure. The composite panels contain the two layers of insulation with the secondary barrier in between. After positioning adjacent composite panels and filling the 3 cm gap, the secondary membrane is spliced together by epoxying an additional overlapping layer of secondary membrane over the joint. All seams are covered so that the secondary membrane is a continuous liner.

The secondary membrane is comprised of a thin aluminum sheet and fiberglass cloth. The fiberglass-aluminum-fiberglass composite is very durable and flexible with an overall thickness of about 1 mm. The secondary membrane is placed within the insulation space. It surrounds the bottom and sides. In the unlikely event of an internal leak from the primary membrane of the cryostat into the insulation space, it will prevent the liquid cryogen from migrating all the way through to the steel support structure where it would degrade the insulation thermal

performance and could possibly cause excessive thermal stress in the support structure. The liquid cryogen, in case of leakage through the inner (primary) membrane will escape to the insulation volume, which is purged with GAR at the rate of one volume exchange per day.

Element	Area (m ²)	k (W/m·K)	ΔT (K)	Heat Input (W)
Base	38	0.0283	205	495
End Walls	75	0.0283	205	973
Side Walls	77	0.0283	205	987
Roof	38	0.0283	205	495
Total				2,945

TABLE II: Heat load calculation for the near detector cryostat (insulation thickness = 0.45 m for all)

Cryostat Configuration

This section describes the configuration of the cryostat only. The TPC is described in Part II, the LAr1-ND CDR. With the intent to minimize the contamination in the gas region, the ullage will be kept cold (< 100 K). A possible way to achieve this requirement is to spray a mist of clean liquid and gaseous argon to the metal surfaces in the ullage and keep them cold, similar to the strategy that was developed for the cool down of the LBNE 35 Ton prototype.

Outer Support Structure

Two types of outer support structures have been evaluated: steel and concrete. With the current cryostat dimensions, the two are similar in cost, but the steel one presents some advantages. The current reference design is a steel support structure with a metal liner on the inside to isolate the insulation region and keep the moisture out. This choice allows natural and forced ventilation to maintain the temperature of the steel within acceptable limits, without the need of heating elements and temperature sensors, otherwise embedded within the concrete. It reduces the time needed for the construction: the structure will be prefabricated in pieces of dimensions appropriate for transportation, shipped to the destination and only assembled in place. Fabrication will take place at the vendors facility for the most part. This shortens the construction of the outer structure on the detector site, leaving more time for completion of the building infrastructure. If properly designed, a steel structure may allow the cryostat to be moved, should that be desired later in the future.

Main body of the membrane cryostat

The sides and bottom of the vessel constitute the main body of the membrane cryostat. They consist of several layers. From the inside to the outside the layers are stainless steel primary membrane, insulation, thin aluminum secondary membrane, more insulation, metal vapor barrier, and steel outer support structure. The secondary membrane contains the LAr in case of any primary membrane leaks and the vapor barrier prevents water ingress into the

insulation. The main body does not have side openings for construction. The access is only from the top. There is a side penetration for the liquid argon pump for the purification of the cryogen.

Top cap

In the current reference design two plates constitute the top cap: plate A and plate B. The stainless steel primary membrane, intermediate insulation layers and vapor barrier continue across the top of the detector, providing a leak tight seal. The secondary barrier is not used nor required at the top. The cryostat roof is a removable steel truss structure that bridges the detector. Stiffened steel plates are welded to the underside of the truss to form a flat vapor barrier surface onto which the roof insulation attaches directly. Depending on the number and size of the penetrations, Plate B may be the primary container for the gaseous argon itself. In that case there will be radiation shields only and no membrane underneath instead of the same polyurethane and membrane configuration as plate A. The truss structure rests on the top of the supporting structure where a positive structural connection between the two is made to resist the upward force caused by the slightly pressurized argon in the ullage space. The hydrostatic load of the LAr in the cryostat is carried by the floor and the sidewalls. Everything else within the cryostat (TPC planes, electronics, sensors, cryogenic and gas plumbing connections) is supported by the steel plates under the truss structure. All piping and electrical penetration into the interior of the cryostat are made through this top plate, primarily through Plate B to minimize the potential for leaks. Studs are welded to the underside of plate A to bolt the insulation panels. Insulation plugs are inserted into the bolt-access holes after panels are mounted. The primary membrane panels are first tack-welded then fully welded to complete the inner cryostat volume.

Table III presents the list of the design parameters for the top of the cryostat.

Cryostat grounding and isolation requirements

The cryostat has to be grounded and electrically isolated from the building. Table IV presents the list of the current grounding and isolation requirements for the cryostat. Figure 5 shows the layout of the top plate grounding.

Leak prevention

The primary membrane will be subjected to several leak tests and weld remediation, as necessary. All (100%) of the welds will be tested by an Ammonia colorimetric leak test (ASTM E1066-95) in which welds are painted with a reactive yellow paint before injecting a Nitrogen-Ammonia mixture into the insulation space of the tank. Wherever the paint turns purple or blue, a leak is present. The developer is removed, the weld fixed and the test is performed another time. Any and all leaks will be repaired. The test lasts a minimum of 20 hours and is sensitive enough to detect defects down to 0.003 mm in size and to a 10^{-7} std-cm³/s leak rate (equivalent leak rate at standard pressure and temperature, 1 bar and 273 K). To prevent infiltration of water vapor or oxygen through microscopic membrane leaks (below detection level) the insulation spaces will be continuously purged with gaseous argon to provide one volume exchange per day. The insulation space will be maintained at 30 mbar, slightly above

Design Parameter	Requirement
Configuration	Removable metal plate reinforced with trusses anchored to the membrane cryostat support structure. Contains multiple penetrations of various sizes and a manhole. Number, location and size of the penetrations TBD. Provisions shall be made to allow for removal and re-welding six (6) times.
Plate/Trusses non-wet material	Steel if room temperature. SS 304/304L or equivalent if at cryogenic temperature.
Wet Material	SS 304/304L, 316/316L or equivalent.
Fluid	Liquid argon (LAr)
Design Pressure	5.0 psig (~ 350 mbar)
Design Temperature	77 K (liquid nitrogen temperature for flexibility)
Inner Dimensions	To match the cryostat
Maximum allowable roof deflection	0.018 m
Maximum static heat leak	< 20 W/m ²
Temperatures of all surfaces in the ullage during operation	< 100 K
Additional design loads	Top self-weight TPC ($\sim 2,300$ kg total, to be distributed over all anchors) TPC anchors (TBD) Live load (488 kg/m ²) Electronics racks (400 kg in the vicinity of the feedthroughs) Services (150 kg on every feed through)
TPC anchors	Capacity: to be determined by the number of anchors (1,000 kg each anchor, if six). Number and location TBD. Minimum 6.
Grounding plate	1.6 mm thick copper sheet brazed to the bottom of the top plate
Lifting fixtures	Appropriate for positioning the top at the different parts that constitute it.
Cold penetrations	Minimum 2. Location and design TBD.
Lifetime	10 years (5 years of run + 5 years of potential upgrade)
Thermal cycles	20 complete cycles (cool down and total warm up)

TABLE III: *Near detector cryostat top requirements*

atmospheric pressure. This space will be monitored for changes that might indicate a leak from the primary membrane. Pressure control devices and safety relief valves will be installed on the insulation space to ensure that the pressure does not exceed the operating pressure inside the tank. The purge gas will be recirculated by a blower, purified, and reused as purge gas. The purge system is not safety-critical; an outage of the purge blower would have negligible impact on LAr purity.

Parameter	Requirement
Isolation	1) The cryostat membrane and any supporting structure, whether it is a steel structure or a concrete and rebar pour, shall be isolated from any building metal or building rebar with a DC impedance greater than 300 k Ω . 2) The outer support structure shall be electrically isolated from the building. 3) All conductive piping penetrations through the cryostat shall have dielectric breaks prior to entering the cryostat and the top plate.
Grounding	1) The cryostat, or detector ground, shall be separated from the building ground. 2) A safety ground network consisting of saturated inductors shall be used between detector ground and building ground. 3) Parameters TBD.
Top Plate Grounding	1) The top plate shall be electrically connected to the outer support structure. Parameters TBD. 2) The top grounding plate shall be electrically connected to the cryostat membrane by means of copper braid connections. <ol style="list-style-type: none"> a) Each connection shall be at least 1.6 mm thick and 63.5 mm wide. b) The length of each connection is required to be as short as possible. c) The distance between one connection and the next one shall be no more than 1.25 m. d) The layout can follow the profile of several pieces of insulation, but it shall be continuous. e) The DC impedance of the membrane to the top plate shall be less than 1 Ω.

TABLE IV: *Near detector cryostat grounding and isolation requirements.*

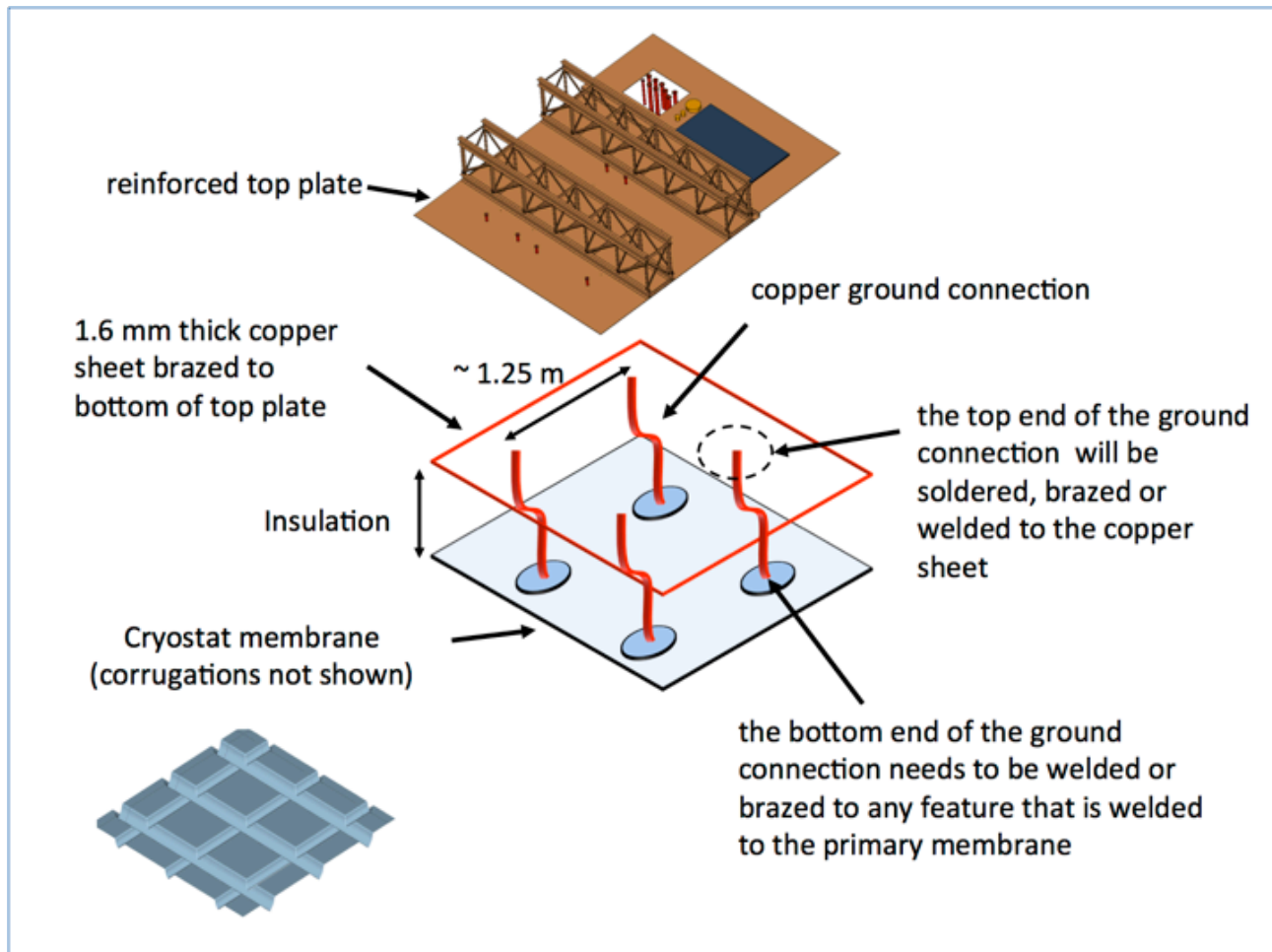


FIG. 5: *Top plate grounding layout for the near detector cryostat.*

B. Far Detector Cryostat

The features of the Far Detector new cryostats and insulation were already described in Part III Section V D. In the following, only a brief summary of the specifications is reported.

New cryostats using a passive polyurethane foam insulation, similar to that used for the membrane cryostat of the near detector, have been designed to house the refurbished T600 detector as shown in Figure 6. The inner cryostats will consist of Aluminum vessels constructed from welded extruded profiles designed by a collaboration between industries and Milano Politecnico (Italy). The vessels are required to be super clean, vacuum-tight and to stand a 1.5 bar maximal operating internal over-pressure. Figure 7 shows a 3D model of the vessel assembly.

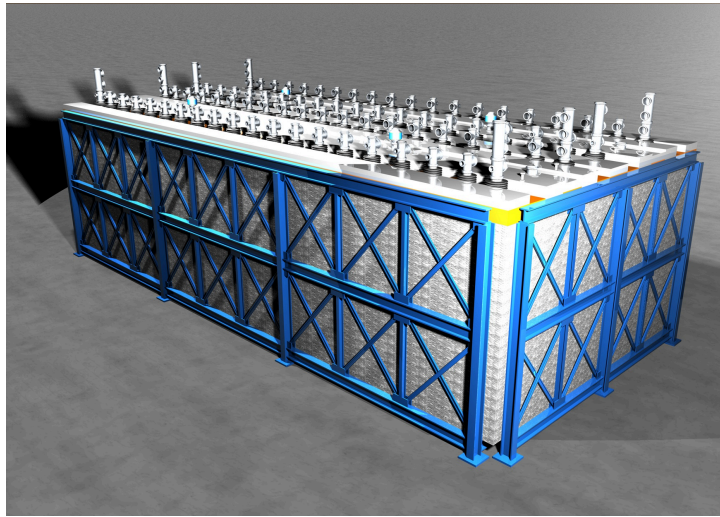


FIG. 6: A 3D model of the T600 detector in new cryostat consisting of new Aluminum inner vessels, polyurethane insulation and outer cryostat.

The inner cryostats will be enclosed in a passive polyurethane foam insulation developed by GTT, similar to that used for the membrane cryostat of the Near Detector, as shown in Figure 8. The foam insulation will be contained in a new outer frame and coupled to boiling-LN₂ cooling shields, used for heat interception. Expected heat loss through the insulation is estimated at approximately 6.6 kW.

Although not described in detail here, the grounding and isolation for the far detector cryostat will need to be handled with the same care as described above for the near detector. The grounding and isolation for the T600 will abide by all Fermilab safety standards.

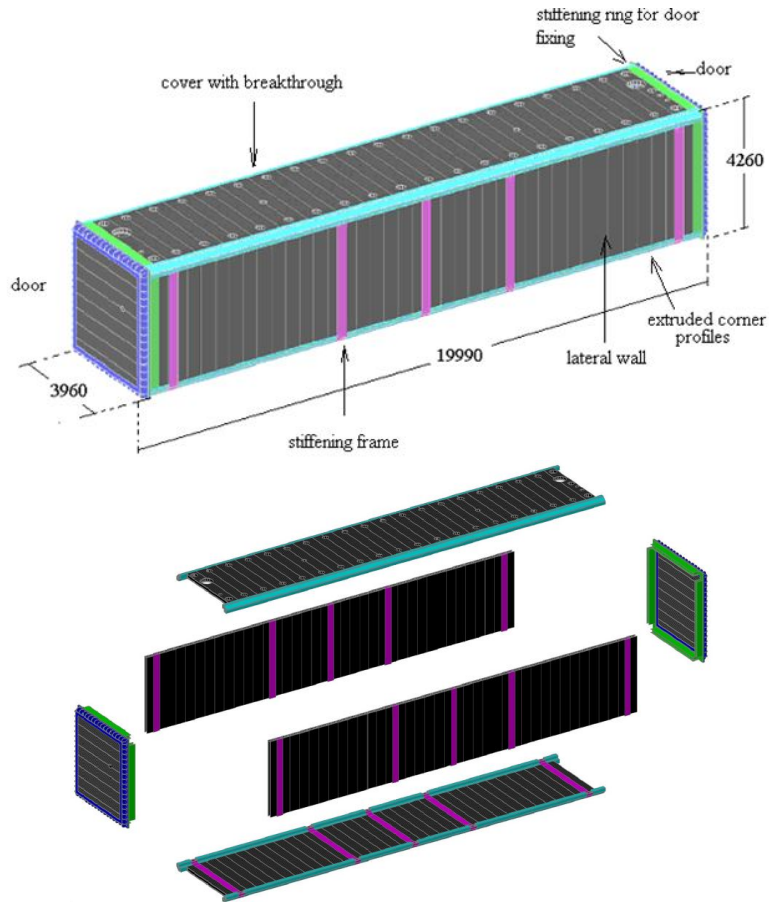


FIG. 7: 3D model of the proposed new Aluminum vessels for the T600 far detector.

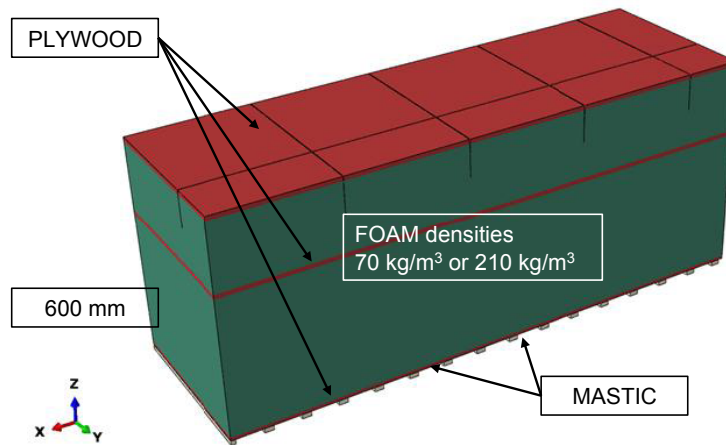


FIG. 8: A 3D model of the insulation for proposed new T600 cryostat. A 600 mm thick element is displayed

III. CRYOGENIC SYSTEMS

The near and far detector cryogenic designs are being developed with a focus on commonalities which can be used across both detectors and also as a stepping stone for LBNF collaborative efforts. These systems will be modular in design and constructed on skids that can be tested separately prior to delivery to Fermilab for installation. Figure 9 outlines the basic LN₂ supply system which is proposed by CERN and agreed as an appropriate solution for both detectors. Each experiment will rely on LN₂ tankers for regular deliveries to local dewar storage. Storage dewars will be sized to provide several days of cooling capacity in the event of a delivery interruption. Note that for the far detector, the original Stirling machines used at Gran Sasso will not be used in the LN₂ cycle. The lower estimated heat leak of the newly designed vessels allows for use of an open loop system typical of other LAr-TPC vessels operated at Fermilab (LAPD, LBNE 35 Ton proto., and MicroBooNE).

Figure 10 shows a schematic diagram of the proposed LAr1-ND liquid argon system. It is based on experience in the design of the LBNE 35 ton prototype and the MicroBooNE detector systems.

Preliminary discussions on the requirements and development of the T600 cryogenic system are ongoing. These discussions include the purification system, best re-condensation strategy, and ullage conditions. It is not expected that these aspects will change significantly from previous experience, where the systems performed well enabling the experiment to achieve very high levels of Argon purity with electron lifetime exceeding 15 ms. A description of the existing T600 cryogenic and purification systems can be found in [1] and the latest results on Argon purity are detailed in [2].

The existing cryogenic system on the ICARUS-T600 detector is therefore meant to be kept as is, apart from the implementation of the open-loop LN₂ delivery system. Figure 11 shows a schematic diagram of the T600 argon system including the existing LN₂ refrigerators. These refrigerators would be replaced by a system like that shown in Figure 9 (bottom).

The responsibility for the design and construction of the cryogenic systems will be shared between CERN and Fermilab, along with INFN, by Liquid Argon Cryogenics groups that have been formed at each laboratory. A preliminary division of the responsibilities by deliverable is outlined in Table V. The schedule for the development of the ND/FD cryogenic systems, cryostats, and detectors is described in Part VI of the proposal.

LAr/GAr System	Service Type	Responsible
LAr Receiving Facility	Cryo	FNAL
LAr/GAr Transfer Lines	Cryo/Non Cryo	FNAL
GAr/H ₂ Supply and Transfer Lines	Non Cryo	FNAL
GAr Filtration	Non Cryo	shared
GAr Analyzers	Non Cryo	shared
Condenser	Cryo	shared
LAr handling and purification System	Cryo	shared
Inside piping	Cryo/Non Cryo	shared
GAr handling system	Non Cryo	shared
LN ₂ System	Service Type	Responsible
LN ₂ Receiving Facility	Cryo	FNAL
LN ₂ Transfer Lines	Cryo	FNAL
GN ₂ returns	Non Cryo	INFN/CERN
LN ₂ /GN ₂ handling system	Cryo/Non Cryo	INFN/CERN
LN ₂ Distribution Facility	Cryo	INFN/CERN
LN ₂ Pumping Station	Cryo	INFN/CERN
Services	Cryo	shared
Ancillary Items	Service Type	Responsible
Process Controls	Non Cryo	FNAL
Design/Drafting	Non Cryo	shared
Smart P&IDs	Cryo/Non Cryo	shared
Safety aspects of cryogenic installation at Fermilab	Cryo	FNAL

TABLE V: Draft proposal for CERN, FNAL and INFN responsibilities, for what concerns the management of the cryogenic system maintenance and on-site logistics. The keyword 'shared' refers to tasks to be undertaken jointly by all groups.

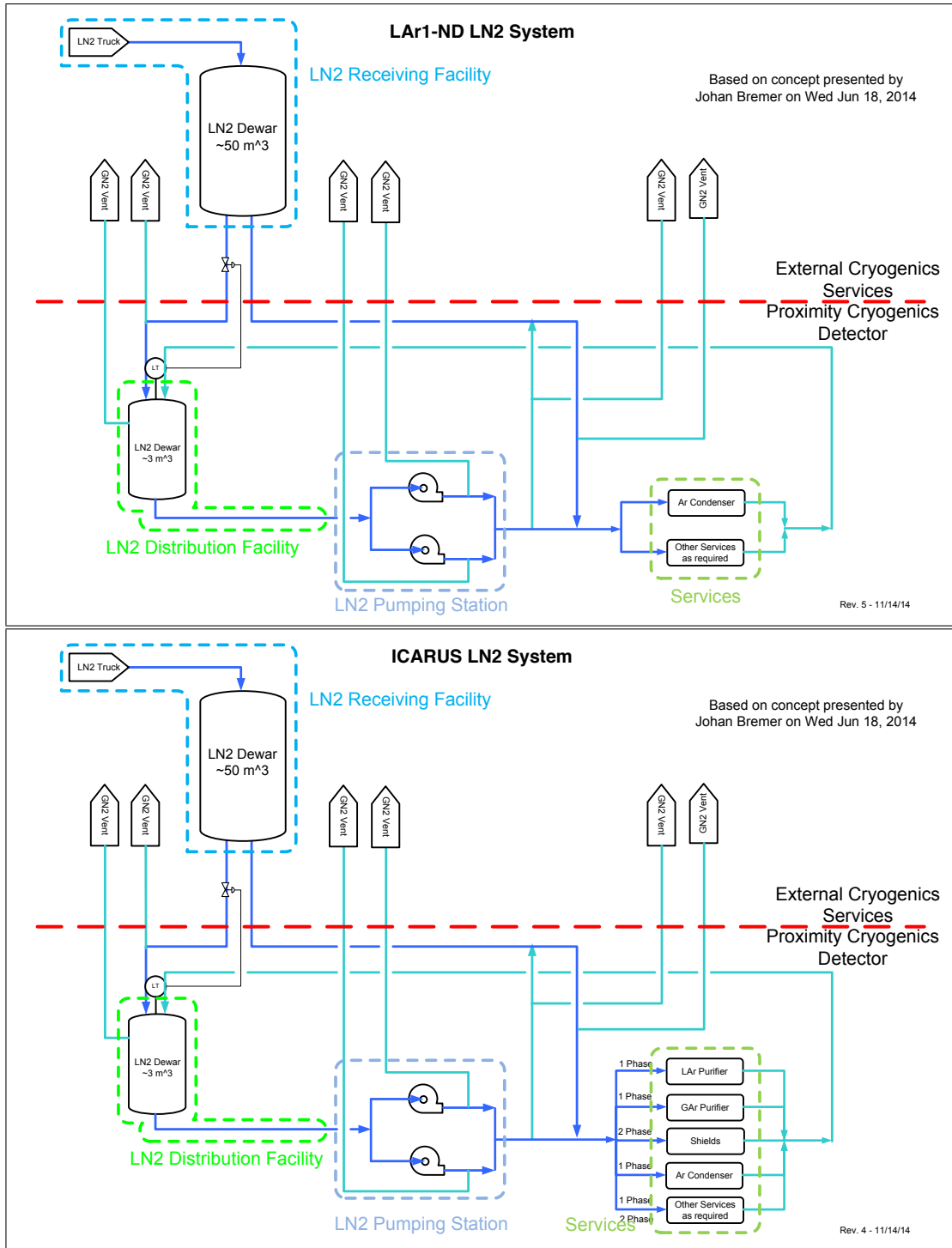


FIG. 9: Schematic diagrams for the proposed LN₂ systems for LAr1-ND (top) and T600 (bottom) detectors.

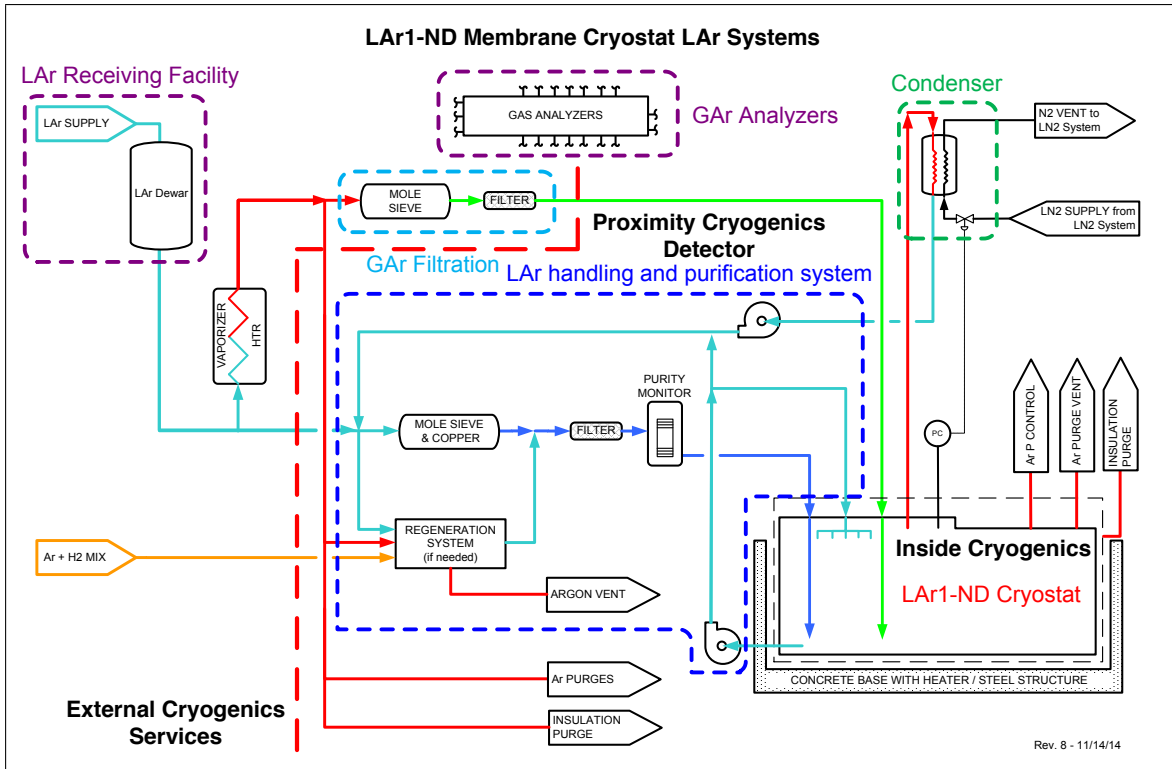


FIG. 10: Schematic diagram for the proposed LAr1-ND liquid argon systems.

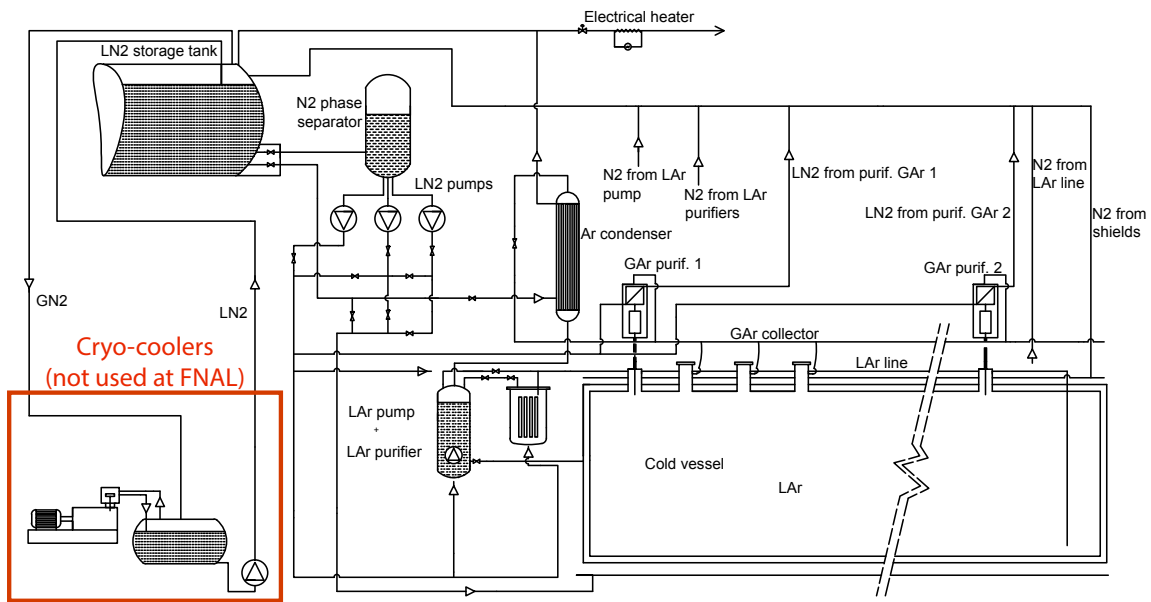


FIG. 11: Schematic diagram of T600 cryogenic system. The section in the lower left would be replaced by the new liquid nitrogen delivery system show in Figure 9.

IV. REQUIREMENTS FOR NEAR AND FAR DETECTOR BUILDINGS

We present preliminary lists of requirements for the far and near detector buildings for support of the cryostats, cryogenics and detector systems. These are shown for example only, the complete list of requirements are contained in separate documents maintained by the Fermilab Engineering Support Services personnel responsible for the building design.

The following is a list of required infrastructure for the cryostat and TPC installation in the near detector building:

- minimum free area around perimeter of cryostat of 0.92 m (per FESHM);
- lay down space equivalent to one cryostat footprint for assembly staging;
- a crane with capacity of 5 ton for cryostat assembly and TPC installation, higher capacity may be needed if TPC is installed with the cryostat top;
- full crane coverage over the cryostat and lay down space;
- minimum hook height above the cryostat 5.75 m (6.0 m if top cap installed with TPC already mounted). Detailed requirements for power and cooling are under development.

The following is a list of key infrastructure requirements to support the installation and operation of the T600 detector in the far detector building:

- a crane with 5/10 ton capacity;
- 300 kW power is needed, to be divided among read-out electronics and cryogenic plant. This evaluation does not include general services as light, ventilation, heating. An UPS will be needed for control and monitoring systems;
- a closed-circuit water cooling system, with flow rate of 5 m³/h, and a pressure/temperature drop of 1.5 bar and 10°C, respectively;
- for safety, separation walls to surround the T600 and cryogenic areas (minimum height 3-4 m), safety sensors (oxygen, smoke, temperature), emergency light, audio alarms;
- for other general services, as no specific requests are needed, the FNAL Standards and Rules will apply, as in the case of Safety Ventilation: two flow rates systems are foreseen, one always running, the other to be started in case of emergency (e.g.: low Oxygen).

For both the near and far detector buildings, the requirement to place concrete blocks for the required overburden will most likely set a higher requirement for the crane capacity.

V. NEAR DETECTOR SITING AND CONSTRUCTION

The location of the near detector building is approximately 110 meters from the existing BNB target located in the MI-12 Building. The new building incorporates conventional facilities to provide the spatial and infrastructure requirements needed to install and operate the components that comprise the near detector. Figure 12 shows a concept for the near detector building in cross section. In general, the construction will consist of a 1,300 square foot (120 m²), below-grade enclosure centered on the existing Booster Neutrino Beam that will house

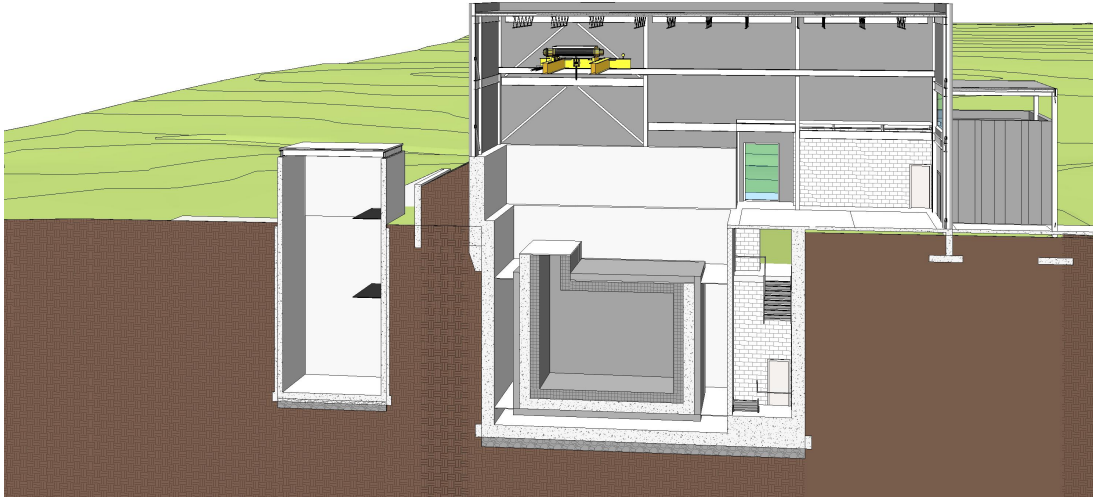


FIG. 12: *Cross-sectional view of a design concept for the building that will house the near detector below-grade. The design includes a surface building. The existing SciBooNE enclosure to the left will be used for the cryogenic system. The beam enters from the left in this view.*

the LAr-TPC and related electronics while the 2,300 square foot (215 m²) above-grade portion will provide a means for staging and installing the detector components as well as personnel access. The site work will include utility extensions from MI-12, cryogenic storage tanks, gravel staging areas and vehicle access to the near detector building. Figure 13 shows an aerial view of the building with the SciBooNE and MI-12 target buildings to the left.



FIG. 13: *Aerial view of design concept of the near detector building.*

This near detector location, north of the existing SciBooNE Detector Enclosure allows the existing SciBooNE enclosure to be re-purposed to provide support space for the cryogenic equipment required to operate the detector. The SciBooNE enclosure can be seen on the left in Figure 12. An alternate solution with the cryogenic equipment located on the surface is under study.

The lower level of the near detector building will house the 220 ton near detector. The detector will be located to align slightly off center horizontally (to the east) of the existing Booster Neutrino Beam, placing the floor of the lower level at elevation 713 feet (217.3 m), or approximately 30 feet (9.1 m) below existing grade. The floor plan of the lower level includes access around the near detector and a stairway to grade. The stairs to grade will include a landing at the top of the detector to provide access to the cryostat and supporting equipment. An opening will be cut into the existing SciBooNE Detector Enclosure at the lower level to allow piping and communication access between the two spaces. The below grade walls and floors will be constructed of cast-in-place concrete and will include a groundwater underdrain system connected to the existing SciBooNE Detector Enclosure sump pump.

The upper level of the near detector building will provide unloading/loading, staging and support space for the construction, assembly and operation of the near detector. The structure will be designed to accommodate a 5 ton capacity overhead bridge crane to unload and transport detector components from the grade level loading dock to the below grade detector enclosure. While not installed initially, the structure will be designed to accommodate the installation of up to 9.84 feet (3 meters) of removable precast shield blocks over the detector. This shielding can be added after detector installation if needed to reduce cosmogenic backgrounds. The surface building will be a steel framed, metal sided building with a cast-in-place concrete foundation.

VI. FAR DETECTOR SITING AND CONSTRUCTION

The new far detector building incorporates the conventional facilities to provide the spatial and infrastructure required to assemble, install, and operate the physics components that comprise the T600 far detector. The location of the far detector building is approximately 600 meters from the existing BNB target just downstream of the existing MiniBooNE experiment building. In general, the construction will consist of a 7,100 square foot (660 m²) below-grade enclosure housing the relocated T600 detector as well as related electronics while the 4,000 square foot (370 m²) above-grade portion will provide a means for staging and installing the detector components as well as personnel access. Figure 14 shows a cross-section view the design concept for the far detector building at the early stages of final design. Figure 15 shows an aerial view of the building with the MiniBooNE hill visible to the right.

The site work for the far detector building will include utility extensions from existing utility corridors, storage tanks, gravel staging areas, and vehicle access to the far detector building.

The lower level of the far detector building is sized to house the T600 detector. The detector will be located to align both horizontally and vertically with the existing BNB, placing the floor of the lower level at elevation 713 feet (217.4 m), or 32 feet (9.7 m) below existing grade. The floor plan of the lower level includes code required access space around the detector as well as space to the north end of the detector for detector support equipment. Surrounding the detector enclosure are several alcoves that will house electronics and support equipment required for detector operations.

The structure will be designed to accommodate a 10 ton capacity overhead bridge crane to unload and transport detector components from the grade level loading dock to the below

grade detector enclosure. The lower level of the building will be designed to accommodate up to 9.84 feet (3 meters) of earth equivalent shielding over the below grade detector enclosure if this is found to be needed to reduce cosmogenic backgrounds. Prior to the installation of the concrete shield blocks, the lower level will be open to the crane bay above. Once the shielding blocks are in place and crane access is not available, a 5,000 pound (2,200 kg) capacity material hoist will be used to transport equipment between the upper and lower levels. The lower level will include two (2) code-compliant exit stairs to grade as well as a duplex underdrain system which will collect groundwater.

The upper level of the far detector building will provide unloading/loading, staging and support space for the construction, assembly and operation of the far detector in addition to the mechanical, electrical and toilet facilities required to operate the building. The surface building will be a steel framed, metal sided building with a cast-in-place concrete foundation. The building will have exposed finishes.

The SBN Far Detector Building will be designed to allow the detector to be installed through removable roof sections.

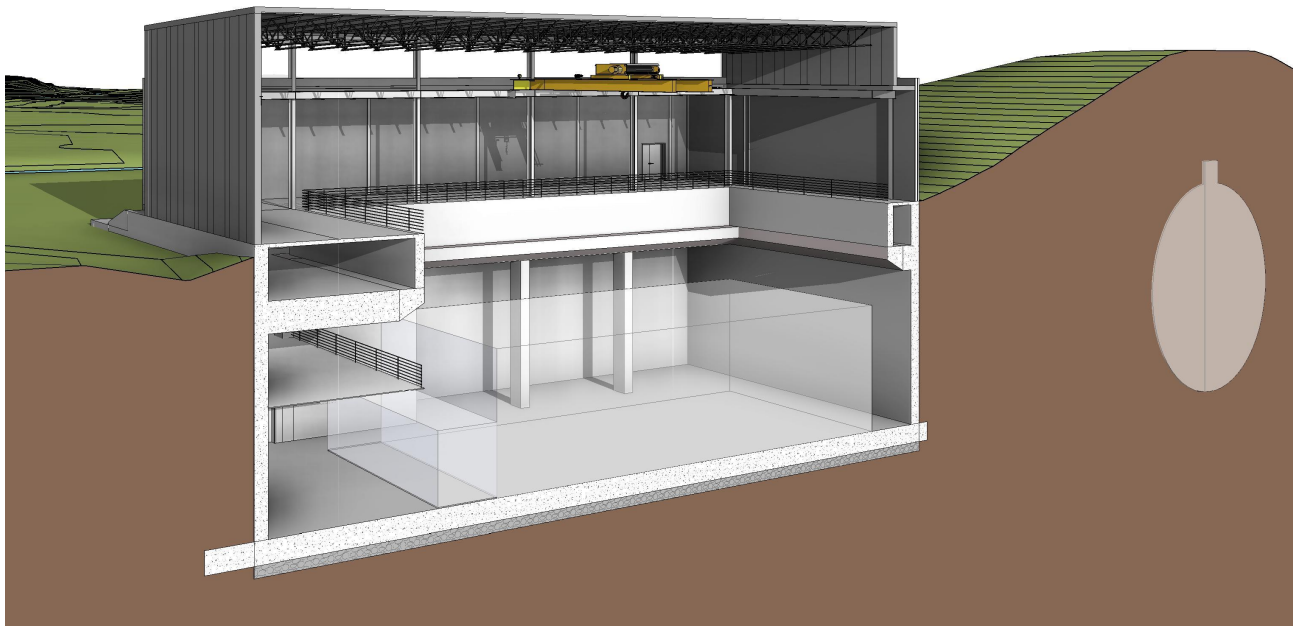


FIG. 14: *Cross-sectional view of a design for the far detector building. The T600 cryostat will be housed in the below-grade portion. Equipment can be lowered into the below-grade area from the surface building using the internal overhead crane. The two T300 TPC modules will be installed through a removal roof section. The beam enters from the right in this view. The MiniBooNE hill is to the right.*

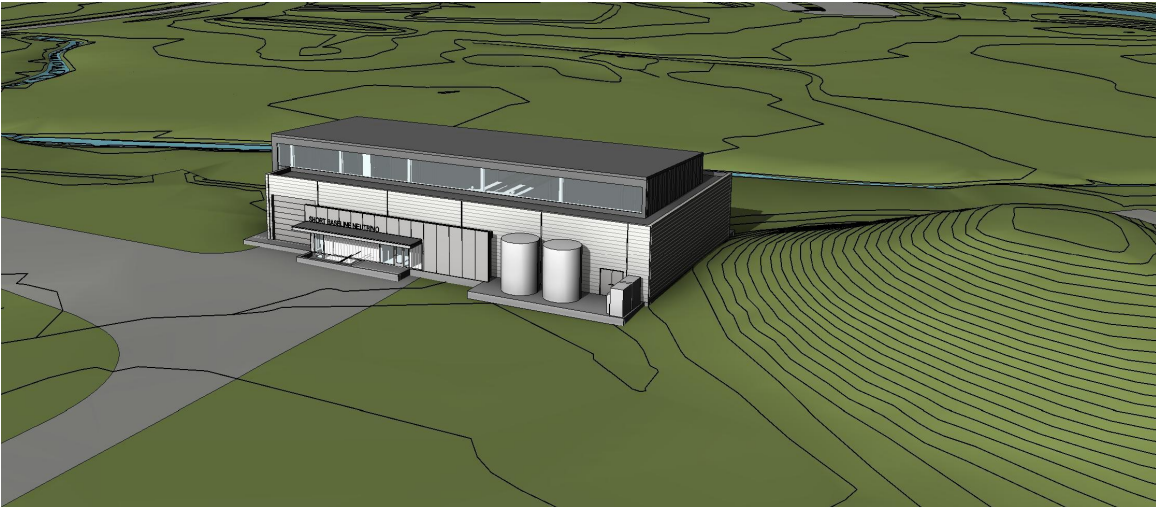


FIG. 15: *Aerial view of design for the detector building.*

VII. COMPUTING INFRASTRUCTURE AND SOFTWARE

The details of the computing needs for the near and far SBN detectors have not yet been fully specified, but it is recognized that the use of similar or identical applications, software libraries, and user interfaces would simplify development, maintenance, and operation. Developing common solutions will be valuable through the full data processing stream from data acquisition software to event reconstruction and analysis. It will not be possible to have completely identical software due to physical differences in the design of the detectors and electronics. However, common frameworks can be used where differences are handled through geometry databases and detector specific versions of some modules. Not only will common solutions result in a more efficient use of scarce programming resources, in a number of places it will be critical to maximizing the sensitivity of the measurements. For example, common reconstruction tools will be needed to ensure that systematic effects between the different detectors can be carefully studied and minimized.

In this section, we outline where common solutions could most benefit the program: data acquisition, data quality monitoring, analysis framework, and reconstruction tools. The description uses several Fermilab support products as examples: the *art* analysis framework, the *artdaq* data acquisition package, and the LArSoft tools interface. We then discuss the current state of automated event reconstruction within the collaborations and plans to advance this critical area in common.

A. Data Acquisition and Data Quality Monitoring

Common data acquisition infrastructure would allow developers and shift crews to more easily switch between the DAQ systems on the different detectors. Of course, the DAQ software can not be completely identical because of differences in the detectors, the readout electronics, and any online analysis needs. However, the use of a common DAQ software framework would provide the benefit of common infrastructure and functionality while supporting experiment-specific customizations.

There are several data acquisition frameworks in use in high energy physics today, including *artdaq* which has been developed by the Scientific Computing Division at Fermilab. As an example of what such a framework provides, *artdaq* includes core functionality in the areas of data transfer, event building, process management, system and process state behavior, control messaging, message logging, and configuration of software and hardware. It also provides online processing and data quality monitoring functionality using the *art* framework which is used in the offline environments of many of the current experiments at Fermilab.

With frameworks such as this, experimenters can focus on the development of the software components that are particular to their experiment. In the case of *artdaq*, this includes the modules that read out and configure the electronics that are used by the experiment. It also includes the reconstruction, filtering, and compression modules that are run online, and the software modules that monitor the quality of the data as it is being acquired. The framework model that is implemented in *artdaq* is shown graphically in Figure 16.

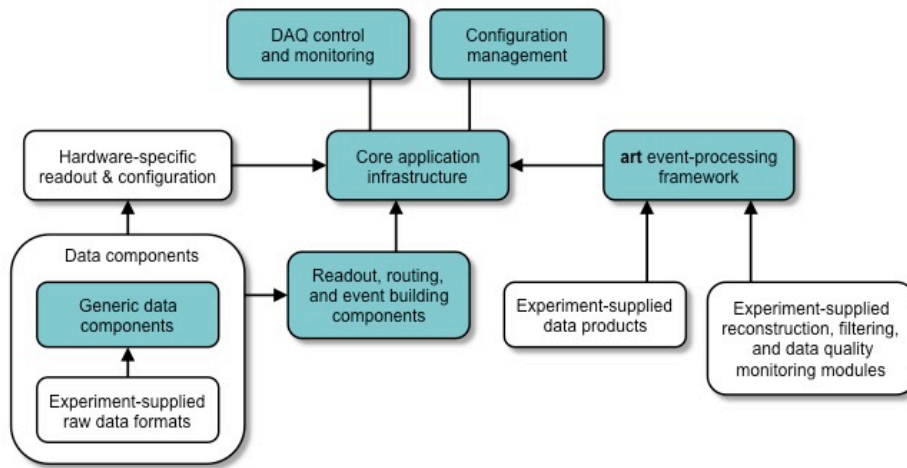


FIG. 16: Sample data acquisition framework architecture, as demonstrated by the *artdaq* toolkit. The blue-shaded boxes show functions that are provided by the framework. The white boxes show the components that are developed by each experiment.

The *artdaq* framework is currently used or will be used by several experiments including the DarkSide-50 experiment, the LArIAT testbeam experiment, the LBNE 35-ton prototype detector, and Mu2e. The benefits of using such a framework has been demonstrated in each of these, most notably the LBNE 35t DAQ in which experimenters from the UK developed the software interfaces to the custom DAQ hardware.

In addition to making maintenance and operation easier, the use of a common DAQ system or framework would allow for coordinated operation, if that would be useful. For example, an umbrella run control application could allow shift operators to *start* and *stop* data taking runs for the SBN detectors simultaneously, even if the internal timing structure of the data and the analysis and storage of the data are independent.

Lastly, the use of a common DAQ framework may provide benefits for software organization. If were useful for the software components that provide convenient access to the raw data for each of the three detectors to be grouped into a single software package, that could be facilitated by the use of a single framework.

The implementation of LAr1-ND experiment-specific items in Figure 16, including low-level hardware access for configuration, control and readout, would benefit greatly from experience with MicroBooNE. Although MicroBooNE does not use *artdaq*, as it was designed prior to its existence, many of the design and control features are common. Also, the LAr1-ND front-end electronics are quite similar to that of MicroBooNE, as shown in Part 3 of this proposal. The FEM (Front End Module) readout boards are quite similar (with the exception of cold digitization in the LAr1-ND case). The Nevis PCIe interfaces to the sub-event computers are identical, allowing much of the lowest level Linux software to be recycled. Since the channel counts and expected neutrino rates at both MicroBooNE and LAr1-ND (11,262 channels) are quite similar, the data throughput requirements and the design of the event builder need not be improved or changed. If *artdaq* is chosen, the lower level readout and control code will have to be integrated into that framework; experience with the successful integration in LArIAT will help in this regard. In *artdaq* nomenclature, there would be one BoardReader process per sub-event computer plus FEM crate.

The ICARUS-T600 detector requires readout of significantly more channels (53,248) which makes a common front-end solution more difficult. However, with the downstream solution shown in Figure 36 of Part 3 of this proposal, with a CAEN A3818 PCIe interface, ICARUS will share a common computer-side sub-event readout bus. One *artdaq* BoardReader per A3818 would match with similar function as with LAr1-ND, one in each sub-event computer. With a cluster of identical sub-event Linux computers forming the first stage of ICARUS event building, we can make the data flow elements downstream of the PCIe bus look essentially identical. Any readout control functionalities will of necessity be distinct from LAr1-ND. Extensive experience with the CAEN A3818 PCIe interface on LArIAT, MINER ν A and CMS experiments would greatly benefit work in this direction. In any choice of framework, whether *artdaq* or other solution, having the frameworks at both ICARUS and LAr1-ND identical will speed development and ease maintenance enormously.

To control all aspects of the items in Figure 16 in a convenient manner for the shift-crew to understand and operate, we will need a Run Control graphical user interfaces (GUI). The MicroBooNE experiment has successfully ported the NO ν A GUIs based on the QT graphics framework for overall Run Control, application control and resource management. As even porting a GUI is difficult and time consuming, ICARUS and LAr1-ND should come up with a common solution to avoid duplication of effort. Behind the scenes of these applications we need a run configuration database to store configuration options and actual configuration used during run time. The *artdaq* group plans to implement such functionalities, and we tag along or follow the MicroBooNE example. In any case, having a similar DAQ architecture at both far and near detectors will simplify all of these issues.

The final element of online software spans the boundary between online and offline analysis: the online data quality monitor (DQM). The DQM process should have fast access to the data as they arrive, in real-time in order that DQM can find problems with the experiment quickly to avoid beam time loss. Depending on the data rates and the processing speed of the DQM process(es), it may not be possible for the DQM process to analyze all of the data in real-time, so a variable prescaling system is needed to, say, process one out of three events, where three can be adjusted so that DQM in no way impedes the main data flow. The DQM input mechanism can be via data files on disk, via a shared memory or via a network event service. The latter option allows the DQM to run anywhere and to not need to access the disk files or shared memory directly. In any scenario, the DQM must never be allowed to cause the data acquisition to slow or stop, so communications between the DAQ and DQM must be flexible and robust. The DQM process normally produces a set of histograms or other

ROOT objects that let the shift-crew and detector experts see the status quickly. To display the histograms, we envision a light-weight interface to the ROOT objects via a web server like <http://if-wbm.fnal.gov> which hosts histogram displays for MINOS, MINER ν A and LArIAT.

B. Data Storage and Processing

At this time, it is difficult to precisely evaluate data sizes for the SBN detectors. We assume that data from the detector will be staged to disk and then to tape for archival storage. New data are assumed to remain on disk until an initial pass of production processing can be performed. Subsequent reprocessing of the data, which can be assumed to occur at least once or twice per year, will draw data from tape with a cache disk front end. Production data will, under ideal circumstances, remain on disk for as long as needed for analysis purposes. At least two complete production passes must be resident on disk at any given time. Additional storage will be needed for testing, staging intermediate results, user analysis and management of production processing.

Monte Carlo data production will consume additional storage. We assume that each pass of data production is accompanied by a complete generation and reconstruction of the production Monte Carlo samples. The statistics in each of the Monte Carlo samples will be approximately ten times that.

The following data model is based upon experience from other neutrino experiments and broad assumptions about data sizes and rates. Given the large uncertainties at this time about the details of the data and the data model required, we attempt to provide an upper bound on the storage that may be required. Even within this estimate, there are large uncertainties that could change the bound by large factors. Nonetheless, it is instructive to work through some reasonable set of assumptions for the data model to see the order of magnitude of the answer. We should also note that storage technologies change. Any reference to a specific technology in the following should be regarded in that light. The important points will be the total data sizes and rates.

Assuming the new DAQ and beamline operates at a maximum rate of 5 Hz with an addition 5 Hz of simultaneous cosmic ray data taking, the expected upper bound of the data rate from ICARUS-T600 is expected to be or order 500 MB/sec. The LAr1-ND detector will contribute an additional 100 MB/sec in this limit. The raw data is assumed to be compressed, but not zero suppressed. The upper bound on the total raw data size over the course of the SBN run would then be about 1 PB.

The signal samples are approximately 10% of the total, so about 100 TB. Since the raw data is compressed, each pass of reconstructed data will be larger than 100 TB. Low level data, however, could be dropped for the production output. Here, we assume that the production data output is 150 TB per full re-processing pass on the final dataset, which is still small on the scale of the total storage needs for the experiment. We assume that the dataset will be re-processed at least twice per year for the three years of data taking, and twice more in the year after data taking, which results in about 6×150 TB, or about 1 PB of production output over the course of the experiments.

For Monte Carlo data, we assume that we will require 10 times the signal statistics, and that Monte Carlo data is twice as large as raw data in order to accommodate truth information. This yields a total size of 2 PB for a full pass of Monte Carlo on the final dataset. If we assume the same number of re-processings, we get approximately 10 PB for the full Monte Carlo sample by the end of the experiment, which obviously dominates the estimated data size.

Summing over all of these datasets, we arrive at an upper bound on the total production data size that is on the order of 10 PB.

Additional disk storage or the equivalent will be required for the following uses:

- Staging raw data from the detector before writing the archiving the data to tape. Ideally, this data will remain on disk until the first pass of production processing is completed, and large enough to weather latencies and downtimes in the production and archival apparatus.
- Staging of data from tape for production data re-processing
- Staging production output data. Ideally, production output will remain on disk until it is no longer needed for analysis. We should assume at that at least two full production passes must be on disk at once.
- Storage associated with production processing, which includes both special purpose staging and large scale production testing
- Storage for smaller analysis datasets and user analysis
- Storage associated with a DOE mandated data management plan

It is difficult to estimates the needs for these categories, but the asymptotic bound assuming the data size estimates above put the size in the area of a few PB.

Existing technologies deployed at Fermilab, such as dCache and Enstore, already operate at the capacities and throughput scales implied by the above data estimates, so should not introduce unknown costs.

CPU:

Given that the development of simulation and reconstruction algorithms are at a very early stage with only limited exposure to real data (only that from ArgoNeuT), it is premature to make estimates of the CPU capacity required to process and analyze the SBN data. Suffice it to say that there must be sufficient processing available to perform the first pass of production processing in real time with data taking, while at the same time that a full production pass on the data is being performed. In order to provide rapid turn around for analysis, a full reconstruction re-processing of the data, including the accompanying Monte Carlo production, should be possible on the time scale of one to three months.

Even knowing the production processing requirements, it is often difficult to estimate the analysis CPU in advance of actual analysis. In many experiments, the analysis CPU dominates the total consumed, while in others, it is comparable to or smaller than the production CPU. In order to enable the construction of sensible CPU demand models, it is important that the data processing and job submission infrastructure used by the SBN experiments provides the capability to track the specific use for any given job. Fermilab supports several systems that provide this capability.

C. Data Analysis Framework and Tools

The *artproduct* supported by Fermilab is a general-purpose data processing framework for offline data production and analysis that is well-suited for use in neutrino and related experiments. A number of experiments have adopted the *artframework*, including NO ν A,

g-2 and Mu2e, as well as the LAr-based experiments ArgoNeuT, MicroBooNE, the former LBNE, LArIAT, and LAr-1ND. The question of using *art* for ICARUS-T600 will be addressed separately later in this section.

The choice of LAr-TPC technology and the consequent similarities in readout geometries across experiments offers a unique opportunity for developing common solutions for the simulation, reconstruction and analysis of data for the experiments. The LArSoft project, a joint venture between the experiments, software providers and Fermilab, supports the development and maintenance of an integrated, *art*-based, experiment-agnostic software suite for simulation, reconstruction and analysis of LAr-TPC data. All of the current LAr-TPC-based experiments at Fermilab are members of LArSoft; Fermilab manages the project. Participating experiments contribute algorithms to the LArSoft suite. By using generic interfaces to the services that provide otherwise detector-specific information, the algorithms can be decoupled from the details of the experiment for which code was originally written. In participating in LArSoft, the member experiments also gain access to the algorithms and tools contributed by other experiments.

Some elements of the offline software necessarily require specific knowledge of the particular experiment. In some cases, the required functionality can be hidden behind interfaces that are sufficiently general to be used for all experiments. In either case, each experiment must develop and maintain this software, which includes the geometry description for the detector, readout electronics simulation and digitization algorithms, interfaces to calibration data, etc. Some fraction of the photon reconstruction software may also need to be experiment specific.

At the present time, MicroBooNE contributes code more quickly than do the other experiments, due largely to the proximity to data taking. As a result, most of the reconstruction and simulation algorithms were developed either by ArgoNeuT, the original LArSoft user, or MicroBooNE. While MicroBooNE has successfully completed 5 Monte Carlo challenges using the LArSoft suite over the past few years, the remaining active experiments, LBNE, LArIAT and LAr-1ND have successfully used the same simulation and reconstruction code, but with their respective detector geometries. Notably, LBNE found that a track merging algorithm designed to fix certain reconstruction pathologies in MicroBooNE was able to fully reconstruct tracks that crossed TPC boundaries. While it is clear that each experiment may require algorithms that are only used in their respective experiments or for specific analyses (something which may be particularly true for the SBN analyses), it is equally clear that the existing LArSoft software provides a strong foundation from which to begin development.

The case of the ICARUS-T600 detector is special in that it comes with a legacy data processing and analysis framework, plus simulation and reconstruction algorithms. The choices from this point are to either port the ICARUS code into LArSoft, port the LArSoft code into the ICARUS framework, or to allow each set of code to evolve independently. Oscillation experiments will benefit from using the same or very similar algorithms across all detectors by offering better control of systematics. We argue that porting the ICARUS code into LArSoft is preferred because it allows the most direct and complete sharing of the experience gained by ICARUS for the benefit of the other experiments including eventually the long baseline program. Porting LArSoft into the ICARUS framework might increase the cost of sharing from ICARUS back to the other LArSoft participants. Leaving each independent raises the cost of sharing in either direction, so would be preferred only in the case that porting is prohibitively expensive.

The problem of porting code from one framework into another presents a number of issues that need to be addressed. In no particular order, these issues include the compatibility between data structures and their relationships to each other and the framework; the dependence of algorithm code on framework-specific features; the compatibility of the analysis-level plug-ins

between the frameworks; and the feature sets available within each of the frameworks. Issues such as build systems and external dependencies need to be resolved as well, but those typically do not present major impediments.

LArSoft has adopted the strategy of framework independence for all of its algorithms and data structures, although implementation is far from complete. If successful, the task of porting the code into another framework reduces to the relatively simple task of writing an interface layer between the framework and the algorithms and data structures. In LArSoft, this layer does little more than interact with the framework to access data structure and other services managed by the framework and hand them in framework-independent forms to the algorithms.

D. Toward an Automated Reconstruction

Reconstruction of events in LAr-TPCs is challenging since the fine-grained tracking and calorimetric aspects of LAr-TPCs provide a large amount of information on each neutrino event. Taking full advantage of this information requires a precise, efficient, and automated event selection and reconstruction package.

Reconstruction algorithms are being developed by all three collaborations. MicroBooNE and LAr1-ND simulation and reconstruction software is in the LArSoft framework, while the ICARUS collaboration has a legacy data analysis and reconstruction framework.

The raw data from LAr TPC detectors consists of signal waveforms from each wire in each of the views (three for all the SBN detectors). The reconstruction of events takes these waveforms as input and proceeds in six steps as outlined below:

1. Hit finding: each of the signal waveforms is analyzed to find pulses that are returned as hits, each representing a time and deposited charge on the analyzed wire. The hits are the basic building blocks for the remaining steps.
2. 2D clustering: a clustering algorithm associates the hits in each view into logical groups called clusters.
3. 3D reconstruction: pattern-recognition algorithms match these two-dimensional (2D) clusters across views to create collections of hits associated with the same three-dimensional (3D) objects. This step can involve splitting or merging 2D clusters to better match candidate 3D groupings.
4. Tracks/showers spatial/calorimetric reconstruction: Candidate 3D objects are passed to track- and shower-reconstruction algorithms to produce collections of tracks and showers.
5. Identification of primary and secondary vertices: vertex reconstruction associates tracks (and showers) to produce the full event. The event is represented as a hierarchical collection of the tracks and showers, starting with the event interaction point, arranged according to the logical structure of the interaction.
6. Particle identification: this is performed via dE/dx versus residual range measurement or decay/interaction topologies (stopping particles identification, photon/electron discrimination).

Individual pieces of the reconstruction chain are already at a good level of development and have been used in the analysis of ICARUS-T600 data in the CNGS beam at Gran Sasso

laboratory and ArgoNeuT data in the NuMI beam at Fermilab. It should be noted that due to the bubble-chamber like quality of LAr-TPC data, visual scanning is a very powerful tool that provides an understanding of many features of neutrino interactions that was possible with other technologies and existing experiments. As described in the following, some of the analyses of the ArgoNeuT data have taken advantage of visual scanning. The relatively small size of the ArgoNeuT data sample has made this possible.

A big effort is ongoing with the goal of optimizing the most challenging parts of the reconstruction, namely merging two-dimensional (2D) views into a three dimensional (3D) picture and reconstructing the interaction vertex. The full chain of event selection and reconstruction is being automated to be ready for the analysis of much larger data samples from MicroBooNE and future LAr-TPC experiments. Monte Carlo simulated events, with the inclusion of detector effects, are of course an essential tool in order to develop and test the algorithms.

Scale of necessary reconstruction

The huge number of beam and cosmogenic events that will be recorded in the three SBN detectors (shown in Table VI) demonstrates the necessity of developing automatic reconstruction tools. It is nonetheless foreseen that subsamples of all event topologies and all electron neutrino candidate events will be visually examined. Table VI contains the expected trigger rates in the active volume, prior to application of any energy or fiducial volume cut. These triggers together with a significant rate of crossing muons and other particles from neutrino interactions outside the active volume will constitute the initial data sample. Differently from Table VI of Part I, here cosmogenic triggers include all event topologies in coincidence with the beam spill, independently from the presence of photons.

TABLE VI: *Expected trigger rates in the active volume for a 6.6×10^{20} protons on target (POT) exposure, delivered in 1.32×10^8 beam spills for LAr1-ND and T600, and for a 1.32×10^{21} POT exposure for MicroBooNE. A significant rate of crossing muons and other particles from neutrino interactions outside the active volume is also expected.*

	LAr1-ND	MicroBooNE	ICARUS
ν_μ CC in active volume (AV)	5.2×10^6	3.4×10^5	5.6×10^5
ν_e CC in AV	3.7×10^4	2.2×10^3	3.5×10^3
ν NC in AV	2.0×10^6	1.3×10^5	2.1×10^5
Cosmogenic triggers	3.0×10^6	1.8×10^6	2.5×10^6

The aim of the automatic reconstruction algorithms will be:

- rejection of cosmogenic events and “in drift time” cosmogenic tracks,
- identification of the neutrino interaction and its classification (CC, NC..), and
- estimation of the neutrino energy.

For the first item, the coupling with the light detection and muon tagging systems will be certainly beneficial.

Reconstruction that enables ν interaction identification involves:

- electron/photon discrimination via initial part of the cascade,

- other discriminating features, e.g. energy in the primary vertex region,
- discrimination between pions and muons.

Identification and reconstruction of the neutrino primary interaction vertex is the first prerequisite for the above tasks. Work in ICARUS software framework has shown that reconstructing the primary vertex requires that the full net of tracks must be reconstructed first (where tracks meet at interaction vertices). From this stage one can search for the primary vertex e.g. by looking for the track directions. Electromagnetic shower reconstruction and identification needs primary vertex reconstruction as well. To identify electron neutrino events it is required to select showers pointing to the primary vertex, validate if the shower is not separated from the vertex and if it is possible to identify the shower as related to single electrons.

Current reconstruction capabilities and planned near term work

Reconstruction algorithms of LAr-TPC data have been largely developed on real data from ArgoNeuT and ICARUS-T600 experiments. The MicroBooNE collaboration is giving a very important contribution continuing the development of most of the reconstruction and simulation algorithms in the LArSoft framework.

ICARUS

Many pieces of the reconstruction are ready in the ICARUS framework. A novel approach is followed for 3D reconstruction [3], that outclasses the standard approach of hit-by-hit matching through common timing. Hit-by-hit is prone to ambiguities (especially for objects developing in a direction perpendicular to the drift direction), to missing matches (i.e. in case of objects developing in a direction parallel to one of the wire orientation) and to position quantization (wire pitch). The ICARUS approach instead performs a global fit of all the three independent views starting from pre-identified 2D “objects” or “clusters”, allowing to overcome the above difficulties. Particle identification via dE/dx is also ready, and tested both on Monte Carlo and real events. It is based on a Bayesian neural network algorithm as described in [4].

The automatic identification of 2D “objects” or “clusters” has also been developed and nearly finalized. It is based on a segmentation algorithm that proceeds from the event periphery towards the center, building segments and vertices. The 2D segmentation is fed to the 3D reconstruction to solve ambiguities. Several 2D-3D iteration steps can be envisaged.

Further work is ongoing for the reconstruction of showers and the automatic identification of the primary vertex.

The ICARUS automatic reconstruction has been tested on a large sample of real CNGS events containing muons produced in the materials upstream of the detector. The reconstruction efficiency was checked against visual scanning and found to be about 90% (this sample contains many tracks parallel to the wire planes, thus with almost constant t_0 along the track, which is a very adverse condition for the reconstruction). Tests on low energy real CNGS neutrino events provided encouraging results.

Reconstruction of fully simulated Monte Carlo event samples at the BNB energy has also been performed and shown to give the same identification efficiency as visual scanning. In this case, the position of the primary vertex has been assumed as given from the simulation.

Full automated reconstruction, including the identification of the primary vertex, has been attempted on a sample of simulated ν_μ CC Quasi-elastic events at 1 GeV. The position of the primary vertex was reconstructed within 3 cm in 92% of the events, out of which 72% resulted to have the correct track multiplicity (zero, one, or more protons depending on final state effects in the interaction). The muon initial direction was reconstructed within 20° in 90% of events, and within 4° in 83% of cases.

The currently available reconstruction algorithms were used to prepare methods for automatic background rejection. Two approaches were studied:

- 3D reconstruction of tracks in order to identify muon tracks crossing the detector. The efficiency was checked on a generation of cosmic muons with the results of 95% tracks correctly reconstructed from the full sample. Improvements are under investigation. Known t_0 was assumed in this study.
- Identification of muon signal and its EM activity in 2D projection of the Collection view. Since the Collection view is the source of the calorimetric and dE/dx measurements, the region in the close proximity to cosmic muons and induced EM activity should be excluded from the signal analysis. Clustering algorithms were used to study the potential of such an approach, obtaining an almost complete background reduction with an estimated few percent loss in fiducial volume.

LArSoft

ArgoNeuT was the first experiment using the LArSoft package to simulate and reconstruct neutrino events collected during a run in the Fermilab's NuMI LE beam at the MINOS near detector hall in 2009-2010. The ArgoNeuT experiment [5], a 240 kg active volume LAr-TPC, collected several thousand ν and anti- ν interactions. Automated event selection has been used to extract different samples of events: 1) CC (anti-) ν_μ events, combining TPC tracking information with the downstream MINOS near detector and 2) events with electromagnetic shower activity in the TPC. Fully automated reconstruction has been used for some analyses, requiring the reconstruction of simple or inclusive topologies, while semi-automated reconstruction procedures, guided by visual scanning have been used for detailed reconstruction of final state event topologies. Individual events have been categorized in terms of exclusive topologies observed in the final state and semi-automated geometrical reconstruction has allowed to reconstruct low energy hadrons (protons with 21 MeV kinetic energy threshold) at the vertex of ν events.

Automated geometrical and calorimetric reconstruction of a high statistics sample of minimum ionizing tracks, through-going muons produced by neutrino interactions upstream the detector, has demonstrated the reliability of the geometric and calorimetric reconstruction in the ArgoNeuT detector [6]. Analyses ν_μ and anti- ν_μ CC inclusive events [7], [8], coherent charged pion production on argon [9] and highly ionizing tracks [10] have been performed through fully automated geometrical and calorimetric reconstruction and particle identification (PID). Analyses requiring the complete reconstruction of the final state kinematics [11] have been performed through semi-automated geometrical reconstruction of protons at the vertex followed by fully automated calorimetric reconstruction and PID. Analyses of the selected samples of events with electromagnetic shower activity in the TPC using semi-automated reconstruction procedures to study of NC π_0 events and electron-gamma separation are expected to be finalized soon.

In LArSoft multiple modules for performing a task using different methods may exist. LArSoft currently contains multiple hit-finding, hit-cluster, and charged-particle-track-finding algorithms. Given the existing common software base, these elements represent a significant reduction in the amount of software that must be developed in order to obtain a full simulation and reconstruction chain. LAr1-ND, for instance, completed the necessary detector-specific elements and ran a complete simulation and analysis chain in significantly less than a month using only two part-time developers. This modularized structure allows for fast, independent development of new algorithms, and seamless incorporation of new and different algorithms into the reconstruction chain. Development and optimization of the different algorithms, test and studies of the performances of automated reconstruction chains are in progress on big samples of MicroBooNE Monte Carlo events.

Because the MicroBooNE TPC is situated near the surface of the earth it experiences significant exposure to cosmic rays, which must be removed during the reconstruction phase. This is facilitated using a two-pass reconstruction. The first pass proceeds through the reconstruction steps 1–3 described above and the results are passed to track reconstruction. The resulting tracks are then analyzed for consistency with the cosmic ray background (aided by the PMT system). Hits associated to tracks identified as coming from cosmic rays are removed from the event. The second pass then runs through all six reconstruction steps using the remaining hits, which are taken to belong to a beam-induced event. Data from MicroBooNE will be very important in order to evaluate the performance of this procedure.

Steps to a joint reconstruction effort

It is recognized that teams from the different experiments need to collaborate on the development of common solutions for the simulation, reconstruction and analysis of data for the combined analysis of the three detector data. The details of this reconstruction software have not yet been fully specified. A workshop dedicated to LAr-TPC event reconstruction to define a common strategy will be organized. As a first step to test the current performance of the already existing LArSoft and ICARUS tools it is proposed that ICARUS atmospheric neutrino data, which are in the energy region of the BNB events are reconstructed with LArSoft tools and ArgoNeuT data are reconstructed with the ICARUS tools.

There is an ongoing effort to merge ICARUS reconstruction algorithms into the common framework of LArSoft. Currently the ICARUS algorithms for clusters and 3D track reconstruction are being adapted to the structure of LArSoft. The reconstruction in the LArSoft framework is implemented as modules that allow to perform various stages of reconstruction. Such a modular approach would allow to use any configuration of algorithms already available in the LArSoft together with algorithms developed in the ICARUS framework. This would allow to verify and test algorithms on data from different liquid argon detectors, as well as give possibility to compare with each other independently developed algorithms.

The development of common computing and software systems for the SBN program will benefit significantly of the use and development of these tools on the soon to come MicroBooNE data.

It is the natural role of Fermilab as the host laboratory to provide and support software infrastructure such as the art, *artdaq*, and LArSoft. For the SBN program to successfully take advantage of these tools, it will be essential that sufficient resources are available from Fermilab to assist in code development, code porting, and user support. This support will be needed in

parallel with the construction and refurbishing of the physical detectors.

-
- [1] C. Rubbia, M. Antonello, P. Aprili, B. Baibussinov, M. Baldo Ceolin, *et al.*, “Underground operation of the ICARUS T600 LAr-TPC: first results,” *JINST* **6**, P07011 (2011), [arXiv:1106.0975 \[hep-ex\]](#).
 - [2] M. Antonello, B. Baibussinov, P. Benetti, F. Boffelli, A. Bubak, *et al.*, “Experimental observation of an extremely high electron lifetime with the ICARUS-T600 LAr-TPC,” (2014), [10.1088/1748-0221/9/12/P12006](#), [arXiv:1409.5592 \[physics.ins-det\]](#).
 - [3] M. Antonello *et al.*, “Precise 3D track reconstruction algorithm for the ICARUS T600 liquid argon time projection chamber detector,” *ArXiv e-prints* (2012), [arXiv:1210.5089 \[physics.ins-det\]](#).
 - [4] K M. Graczyk, P. Plonski, and R. Sulej, “Neural Network Parameterizations of Electromagnetic Nucleon Form Factors,” *JHEP* **1009**, 053 (2010), [arXiv:1006.0342 \[hep-ph\]](#).
 - [5] C. Anderson *et al.* (ArgoNeuT Collaboration), “The ArgoNeuT detector in the NuMI low-energy beam line at Fermilab,” *Journal of Instrumentation* **7**, P10019 (2012).
 - [6] C. Anderson *et al.* (ArgoNeuT Collaboration), “Analysis of a Large Sample of Neutrino-Induced Muons with the ArgoNeuT Detector,” *JINST* **7**, P10020 (2012), [arXiv:1205.6702 \[physics.ins-det\]](#).
 - [7] C. Anderson *et al.* (ArgoNeuT Collaboration), “First Measurements of Inclusive Muon Neutrino Charged Current Differential Cross Sections on Argon,” *Phys. Rev. Lett.* **108**, 161802 (2012).
 - [8] R. Acciarri *et al.* (ArgoNeuT Collaboration), “Measurements of Inclusive Muon Neutrino and Antineutrino Charged Current Differential Cross Sections on Argon in the NuMI Antineutrino Beam,” *Phys.Rev.* **D89**, 112003 (2014), [arXiv:1404.4809 \[hep-ex\]](#).
 - [9] R. Acciarri *et al.* (ArgoNeuT Collaboration), “First Measurement of Neutrino and Antineutrino Coherent Charged Pion Production on Argon,” *Phys. Rev. Lett.* **113**, 261801 (2014).
 - [10] R. Acciarri *et al.* (ArgoNeuT Collaboration), “A study of electron recombination using highly ionizing particles in the ArgoNeuT Liquid Argon TPC,” *JINST* **8**, P08005 (2013), [arXiv:1306.1712 \[physics.ins-det\]](#).
 - [11] R. Acciarri *et al.* (ArgoNeuT Collaboration), “Detection of back-to-back proton pairs in charged-current neutrino interactions with the ArgoNeuT detector in the NuMI low energy beam line,” *Phys. Rev. D* **90**, 012008 (2014).